Altermagnetic topological insulator and the selection rules

Hai-Yang Ma [1,*] and Jin-Feng Jia [1,2,3,4]

[1]*Quantum Science Center of Guangdong-Hong Kong-Macao Greater Bay Area, Shenzhen 518045, China*

[2]*Key Laboratory of Artificial Structures and Quantum Control (Ministry of Education), TD Lee Institute, School of Physics and Astronomy, Shanghai Jiao Tong University, 800 Dongchuan Road, Shanghai 200240, China*

[3]*Hefei National Laboratory, Hefei 230088, China*

[4]*Department of Physics, Southern University of Science and Technology, Shenzhen 518055, China*

Altermangetism is newly identified as the third fundamental class of collinear magnetism with zero net magnetization while hosting spin-split bands which break the time-reversal symmetry and Kramers degeneracy. Here, we propose a $\mathbf{k} \cdot \mathbf{p}$ model for a two-dimensional altermagnetic lattice, in which instead of neglecting them, the spin-orbit couplings play the role of driving the system into a topological insulating region. We term this topological phase as an altermagnetic topological insulator, as opposed to an antiferromagnetic topological insulator such as $MnBi_2Te_4$. A spin Chern number is attributed as the topological invariant. We also derive the selection rules for optical conductivity measurements based on our minimal model, with which the elliptically polarized lights will serve as powerful probes to detect altermagnetism and excite individual spin degrees of freedom of altermagnetic compounds through light-induced anomalous Hall effects and longitudinal spin currents.

I. INTRODUCTION

Altermagnetic (AM) materials [1–4] are antiferromagnetic (AFM) but different from conventional AFM compounds whose Kramers degeneracy is conserved even though the time-reversal symmetry ($\mathcal{T}$) is broken. The alternately arranged sublattices in AM compounds having opposite magnetization are related by a crystal-rotation symmetry operation [2,3] and host alternately spin-split bands in the momentum space. This property makes the AM materials very promising in application to spintronics [2]. Specifically, when combined with the valley degrees of freedom (DOF), the spin then would possess a much longer coherence time, which makes the AM materials very suitable in application to quantum computations. Such AM compounds are the so-called $\mathcal{C}$-paired spin-valley locking materials [5].

As a newly identified class of fundamental collinear magnetism, altermagnetism has attracted much attention recently. After its establishment, there have been many theoretic studies [6–39]. Many interesting phenomena such as the anomalous Hall effect [22,40–42], anisotropic crystal thermal Hall effects [43], etc., have been associated with the AM materials. On the experimental side, nonrelativistic spin splitting has been observed by angle-resolved photoemission spectroscopy (ARPES) measurements [44–48]. However, the relativistic spin-orbit coupling (SOC) effects in AM materials are in general not essential for the alternately spin splitting of the energy bands since it is mainly induced by an internal Zeeman field but not SOC. But this does not mean that SOC plays no role in those kinds of materials. Instead, it may lead to interesting

physics such as topological superconductivity [10]. On the other hand, some AM materials are naturally doublet systems, hence, they are very suitable in applications to spintronics, quantum computations, etc. However, doublet quantum DOF are degenerate in energy as required by symmetry. Then, the methods of how to trigger the coupled sublattice-spin DOF are essential in utilizing these AM materials. A naive idea is to lower the symmetry, thus breaking the degeneracy of the coupled sublattice-spin DOF, leaving one of the flavors easily accessible [5]. Regarding this, the lowering operations are expected to be reversible so that the access is repeatable. However, such requirements are not easy to fulfill in real implementations.

In this paper, we first develop a theoretical $\mathbf{k} \cdot \mathbf{p}$ model for a two-dimensional AM lattice at the Brillouin zone (BZ) center starting from a symmetry analysis. By tuning the strength of SOC, the lattice would transit into a quantum spin Hall (QSH) insulator state while having no Kramers degeneracy for a general k point in the BZ. Thus, it is different from an antiferromagnetic topological insulator [49–53]. We call this topological state emerging in the AM material as an altermagnetic topological insulator (AMTI). By analyzing the Chern number for each spin part of the model, we demonstrate that a spin Chern number [54] can be defined as the topological invariant. We then derive the optical selection rules. Additionally equipped with these rules, one can easily identify the altermagnetism and trigger the spin excitations in an AM material through light irradiation, which are not easy tasks in experiments provided that no such selection rules exist. In addition, we demonstrate that there exist light-induced anomalous Hall effects and longitudinal spin currents. These properties not only make the AM materials easily accessible to experiments and suitable to be

---

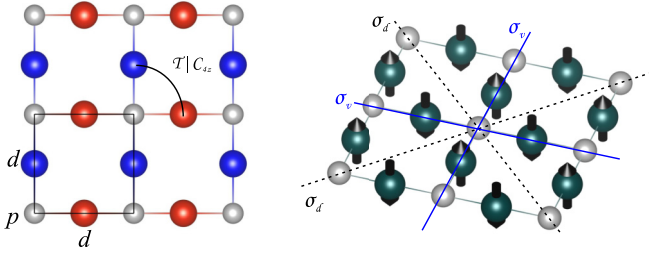*Contact author: mahaiyang@quantumsc.cn

FIG. 1. Schematic of the model 2D altermagnetic lattice. Some essential symmetry operations are illustrated, where $\sigma_{v/d}$ is the mirror plane.

applied in spintronics, but also fascinating by themselves in physics.

II. k · p MODEL

We consider a two-dimensional lattice which lies on an xy plane and consists of three atoms (see Fig. 1). Two magnetic atoms lie at the edge center and the paramagnetic atom lies at the corner within a unit cell. This lattice has been adopted frequently in recent works (see Refs. [5,11,18]). The magnetic atoms can be 3d transition metals, while the paramagnetic atom may be a heavy element such as Te to give sizable SOC. The local magnetic moments of the two magnetic atoms are opposite and directed perpendicular to the atomic plane, or the **z** axis (see Fig. 1). Paramagnetic atoms are essential in setting the altermagnetism, in that they prevent any trivial symmetry operation that exchanges the two alternated sublattices.

We then analyze the symmetry. Before invoking the altermagnetism, the proper wallpaper point group of the non-magnetic lattice is C_{4v}. We focus on the Γ point of the BZ, where we are going to derive our **k · p** model. The Γ point has full point group symmetry C_{4v}. Under the crystal fields brought by the lattice, the fivefold degenerate d orbitals would split according to the irreducible representations of C_{4v}. There are three nondegenerate $d_{z^2}(A_1)$, $d_{xy}(B_2)$, $d_{x^2-y^2}(B_1)$ orbitals and a doublet $[d_{xz}, d_{yz}](E)$ orbital. Similarly, the p orbitals would split into a nondegenerate $p_z(A_1)$ orbital and a doublet $[p_x, p_y](E)$ orbital. Ignoring the mixing between the p-d orbitals, we can pick up two different combinations over them to give the Hamiltonian terms linear in **k**: (1) d_{xy}, p_x, p_y and (2) p_z, d_{xz}, d_{yz}.

We then restore the altermagnetism. Without SOC, the local magnetic moments are free to rotate in real space, so the spin space group is more suitable for describing the symmetry [3,55–57]. Provided that the two magnetic atoms have opposite magnetic moments, the altermagnetism is well established. However, when SOC is included, we should restrict the symmetry operations to the magnetic group, which is only a small portion of the full spin space group. The local moments then can only be taken along the out-of-plane direction if it is necessary that the number of symmetry operations does not change. Restricted by this setting [39], half of the point group symmetries still leave the magnetic lattice invariant, while the other half need to be combined with $\mathcal{T}$ to give the proper symmetry operations. The magnetic group is $C_{4v}(C_{2v})$. Considering the alternated

spin splittings of the energy bands brought by the effective Zeeman field, the basis for a minima four-band model can be taken as (1) $d_{xy\uparrow}$, $\frac{1}{\sqrt{2}}(p_x + ip_y)_\uparrow$, $d_{xy\downarrow}$, $\frac{1}{\sqrt{2}}(p_x - ip_y)_\downarrow$ and (2) $p_{z\uparrow}$, $\frac{1}{\sqrt{2}}(d_{xz} + id_{yz})_\uparrow$, $p_{z\downarrow}$, $\frac{1}{\sqrt{2}}(d_{xz} - id_{yz})_\downarrow$, and all other higher-energy bases are assumed to be integrated out. Under such bases, the two-dimensional (2D) inversion operator C_{2z} has the matrix form $\sigma_0 \otimes \tau_z$, the σ_d mirror symmetry $-i\sigma_y \otimes \tau_0$, the $\{\mathcal{T}|C_{4z}\}$ symmetry $-i\sigma_y\mathcal{K} \otimes \tau_0$ and **k · p**, and the $\{\mathcal{T}|\sigma_v\}$ mirror symmetry is $\sigma_0 \otimes \tau_{x(y)}\mathcal{K}$. The **k · p** Hamiltonian that fulfills these symmetry constraints is read as

$$H(\mathbf{k}) = \epsilon_0(\mathbf{k})I_{4\times4} + \begin{pmatrix} M(\mathbf{k}) & Ak_- & 0 \\ Ak_+ & -M(\mathbf{k}) & 0 \\ 0 & 0 & k_x \leftrightarrow k_y \end{pmatrix}, \quad (1)$$

with $\epsilon_0(\mathbf{k}) = C - D(k_x^2 + A_2^2 k_y^2)$, $M(\mathbf{k}) = M - B(k_x^2 + A_2^2 k_y^2)$, $k_\pm = k_x \pm iA_2 k_y$, where A, A_2, B, C, D, M are constants. In arriving at the Hamiltonian, information of the chemical potential, on-site energies, effective Zeeman (or Kondo-like) couplings, and the atomic SOC are condensed into C and the mass term M. When tuning SOC, the M changes. Note that in our model the anisotropic parameter A_2 is the same for both the linear and quadratic terms; this is in general not the case for real materials, so we wrote it to be so only for convenience in the derivations. We also omit the ϵ_0 term since it is not important in the following discussions.

The Hamiltonian (1) is quite similar to the Bernevig-Hughes-Zhang (BHZ) model for 2D QSH [58]. One difference is that in our model, the linear terms are anisotropic with $A_2 \neq 1$. The other difference is that the lower block is no longer a $\mathcal{T}$ counterpart of the upper block but instead an alternated term. In spite of these two differences, the two models have quite similar properties. Typical band structures of our model are shown in Fig. 2. As we can see in Fig. 2(a), the spin-up and spin-down bands are alternatively dispersed with respect to the Γ point and become degenerate along the mirror line Γ-M. A gap is opened by the mass term M, and depending on the value of M, the model may or may not be a topological insulator. The alternated properties can be better viewed in the 3D band structures as shown in Fig. 2(b). To demonstrate the band anisotropy introduced by A_2, we further plot the constant energy contour in Fig. 2(c), from which we can clearly find that the spin-up (spin-down) valley is an ellipse with the long side along the **x** (**y**) direction, namely, the bands are highly anisotropic. With the Hamiltonian at hand, we then study the topological properties and the optical selection rules.

III. TOPOLOGICAL PROPERTIES

In our model Hamiltonian (1), we can see that the spin-up and spin-down parts are not coupled, even with SOC. As a result, we can calculate the Chern number $\mathcal{C}$ or the Hall conductivity for each spin part with

$$\sigma_{xy} = \frac{e^2}{\hbar}\mathcal{C} = -\frac{e^2}{\hbar}\frac{1}{2\pi}\iint dk_x dk_y f(\mathbf{k})\Omega_{xy}(\mathbf{k}), \quad (2)$$

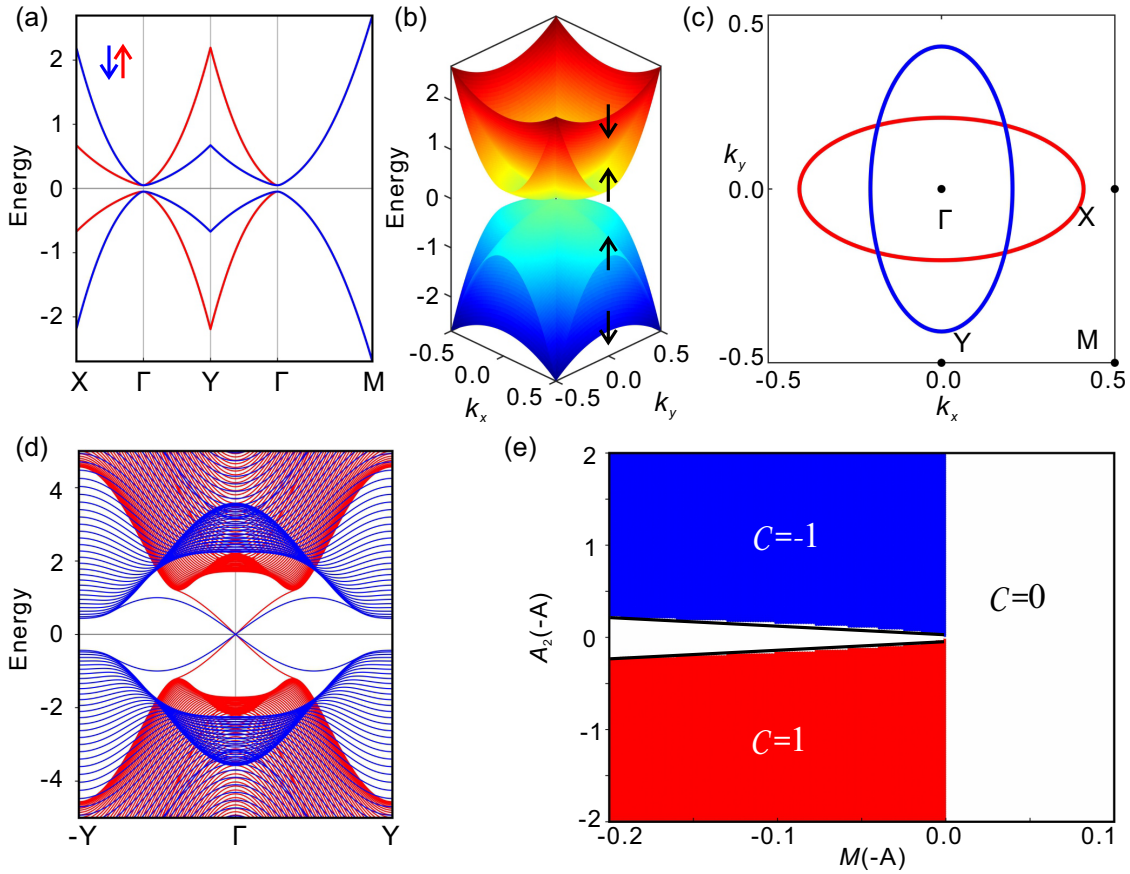$$\Omega_{xy}(\mathbf{k}) = \frac{A^2 A_2 d_3 + 2BA_2(d^2 - d_3^2)}{2d^3}, \quad (3)$$

FIG. 2. Band structures, edge states, and phase diagram. (a) Bands along the high-symmetry path of the $\mathbf{k} \cdot \mathbf{p}$ model, where the parameters are taken as $A = -1$, $A_2 = 2$, $B = -2$, $M = -0.05$. (b) 3D band structures, where the spin is indicated by black arrows. (c) Constant energy contour of the bands, taken at $E = 0.5$. (d) Helical edge states, calculated by directly casting the $\mathbf{k} \cdot \mathbf{p}$ into a pseudolattice, with parameters taken as $A = -1$, $A_2 = 1.3$, $B = -1$, $M = -0.2$. (e) Phase diagram of the pseudolattice model of the spin-up parts, where the model is topologically nontrivial when $M < 0$ and $|M| > 4A_2^2$. The phase boundaries at $|M| = 4A_2^2$ are indicated by black lines, and the other parameters are taken as $A = -1$, $B = A$.

where $d_1 = Ak_x$, $d_2 = AA_2 k_y$, $d_3 = M(\mathbf{k})$, $d = \sqrt{d_1^2 + d_2^2 + d_3^2}$ for the spin-up part. $f(\mathbf{k})$ is the Fermi-Dirac function and $\Omega_{xy}(\mathbf{k})$ is the Berry curvature. Neglecting the quadratic terms at low energy, the Chern number is given by $\mathcal{C} = \frac{\text{sgn}(M)}{2}$, which is a half integer but not an integer since we integrate over a noncompact space [58]. We may understand the results by looking at the gap-closing-and-reopening transition, where M goes from positive to negative, so the Chern number changes by an integer. At the start, the lattice is trivial with $\mathcal{C} = 0$, and by tuning the SOC or the M, the topological transition happens with a nontrival Chern number [58]. The spin-down part can be obtained by noting that $\Omega_{yx} = -\Omega_{xy}$, therefore, the total Chern number is zero. However, the spin Chern number [54] $\mathcal{C}_s = (\mathcal{C}_\uparrow - \mathcal{C}_\downarrow)/2 = 1$ is nontrivial, which indicates that there are chiral edge states for each spin part, similar to the QSH [58,59]. It is easy to check for the existence of chiral edge states. Following Ref. [58], for the spin-up (spin-down) part, we pick a boundary between a low-energy Dirac Hamiltonian with positive mass and one with negative mass. Searching the zero-energy solution, we have $E = Ak_x$ $(-AA_2 k_x)$ for

the edge states when the boundary is parallel to the **x** axis and $E = AA_2 k_y$ $(-Ak_y)$ when the boundary is parallel to the **y** axis. To be more concrete, we put the $\mathbf{k} \cdot \mathbf{p}$ model into a pseudolattice and numerically calculate the edge states and the Chern number of the spin-up part, so the spin Hall conductivity then is $\sigma_s = \mathcal{C}_s e/(2\pi)$, where the results are shown in Figs. 2(d) and 2(e). We can see clearly from Fig. 2(d) that there exist helical edge states, a characteristic of the QSH effect. In Fig. 2(e), we plot the phase diagram of the pseudolattice model with respect to the SOC (M) and anisotropy factors (A_2), from which we find a phase boundary at $M = 0$ and $|M| = 4A_2^2$. When M or A_2 was tuned across the phase boundary, a topological phase transition happens, consistent with the results of the $\mathbf{k} \cdot \mathbf{p}$ model.

We thus obtain a 2D topological insulator which does not have Kramers degeneracy for a general k point. Also, a spin Chern number can be endowed as the topological invariant. The SOC are essential in driving the topological transition which cannot be neglect in this system. Being AM, which is different from antiferromagnetic topological insulators, we therefore call it an altermagnetic topological insulator (AMTI).
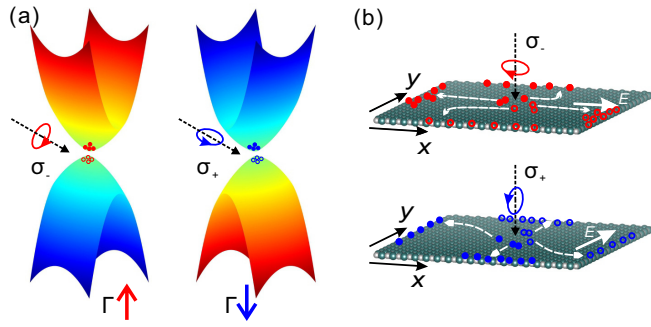
FIG. 3. Schematic of the optical selection rules, light-induced anomalous Hall effect, and longitudinal spin current. (a) Elliptically polarized light $\sigma_-(+)$ would couple dominantly to the spin-up (spin-down) part and the excite out spin-up (spin-down) electron (solid circles) and hole (open circles) carriers on the sample. (b) Light-induced anomalous Hall effect and longitudinal spin current: The top (bottom) panel is for the $\sigma_-(+)$ elliptically polarized light.

IV. SELECTION RULES

To overcome the difficulties of triggering the individual spin DOF of a AM compound, in this section we propose that similar to the $\mathcal{T}$-paired spin-valley-locking materials group-VI dichalcogenides [5,60], one can use elliptically polarized light to excite the single sublattice-spin DOF of the doublet system of our model. The coupling strength to the optical field is $P_\alpha(\mathbf{k}) = m_0\langle u_v(\mathbf{k})|\frac{1}{\hbar}\frac{\partial \hat{H}}{\partial k_\alpha}|u_c(\mathbf{k})\rangle$, $\alpha = x, y$. For the transition near the Γ point, we neglect the quadratic term. The coupling strength with optical fields of $\sigma_\pm$ elliptical polarization then is given by

$$|A_2 P_x \pm iP_y|^2 = \frac{m_0^2 A^2 A_2^2}{\hbar^2}\left(1 \mp \frac{M}{\sqrt{M^2 + A^2|k_+|^2}}\right)^2 \quad (4)$$

for the spin-up part, and

$$|P_x \pm iA_2 P_y|^2 = \frac{m_0^2 A^2 A_2^2}{\hbar^2}\left(1 \pm \frac{M}{\sqrt{M^2 + A^2|k_-|^2}}\right)^2 \quad (5)$$

for the spin-down part. If setting $A_2 = 1$, Eqs. (4) and (5) reduce to the results for group-VI dichalcogenides [60]. However, in group-VI dichalcogenides, the two valleys are well separated in BZ [60], while in our model they merge into one at the Γ point. Second, in our model, A_2 not only gives rise to altermagnetism but also leads to additional anisotropy. Near the BZ center, $M \gg k^2$, therefore, the interband transitions couple dominantly to the $\sigma_- = A_2 P_x - iP_y$ ($\sigma_+ = P_x + iA_2 P_y$) elliptically polarized light for the spin-up (down) part, as illustrated in Fig. 3(a). In the limited case where $A_2 = 0$ or ∞, the interband transitions would couple exclusively to linearly polarized light with $\mathbf{y}(\mathbf{x})$ linearity for the spin-up (spin-down) part. These selection rules are a generalization of

those proposed in Ref. [60]. The anisotropic property also has physical effects. As shown in Fig. 3(b), if we use σ_- (σ_+) light to irradiate the sample to excite the hole and electron carriers, which are then dissociated by an in-plane electric field $\mathbf{E}$, the leading longitudinal spin current signal would be obtained if measured along $\mathbf{x}(\mathbf{y})$. The excited charge carriers will also acquire opposite transverse velocities because the conduction bands and valence bands have opposite Berry curvature, so they will move to the two opposite boundaries of the sample, leading to anomalous Hall currents. Such measurements can point to the existence of altermagnetism if one can determine the spin polarization of the signals, regardless if the compound is topological trivial or nontrivial, and also provide an easy and cheap way to trigger the individual spin DOF of the altermagnetic materials, which is essential for applications.

V. CONCLUSIONS

To conclude, we developed a $\mathbf{k} \cdot \mathbf{p}$ model for a 2D AM lattice starting from a symmetry analysis. With this model we show that by tuning the SOC, the AM material may become topological nontrivial with QSH effects such as a conventional QSH insulator while breaking the Kramers degeneracy for a general point in BZ [58,59]. A spin Chern number was associated as the topological invariant. We further demonstrate that there exist selection rules for elliptically polarized light of our model, which make light irradiation a cheap and powerful method in probing and tuning the AM materials. In addition, we show that there are light-induced anomalous Hall effects and longitudinal spin currents of upon shining the sample with a particular polarized elliptical light. These interesting effects of the AM materials have great potential applications in spintronics [2,3] and sensors [61] and deserve attention in theory. We can see that by coupling the band topology to the altermagnetism, more fascinating physics and phenomena are possible for AM materials. We finally remark that our model can be applied to a Ti_2Te_2O single layer [62].

[1] L. Šmejkal, A. B. Hellenes, R. González-Hernández, J. Sinova, and T. Jungwirth, Giant and tunneling magnetoresistance in unconventional collinear antiferromagnets with nonrelativistic spin-momentum coupling, Phys. Rev. X **12**, 011028 (2022).

[2] L. Šmejkal, J. Sinova, and T. Jungwirth, Beyond conventional ferromagnetism and antiferromagnetism: A phase with nonrelativistic spin and crystal rotation symmetry, Phys. Rev. X **12**, 031042 (2022).

[3] L. Šmejkal, J. Sinova, and T. Jungwirth, Emerging research landscape of altermagnetism, Phys. Rev. X **12**, 040501 (2022).

[4] I. Mazin and The PRX Editors, Altermagnetism—A new punch line of fundamental magnetism, Phys. Rev. X **12**, 040002 (2022).

[5] H.-Y. Ma, M. Hu, N. Li, J. Liu, W. Yao, J.-F. Jia, and J. Liu, Multifunctional antiferromagnetic materials with giant piezomagnetism and noncollinear spin current, Nat. Commun. **12**, 2846 (2021).

[6] L. Šmejkal, R. González-Hernández, T. Jungwirth, and J. Sinova, Crystal time-reversal symmetry breaking and spontaneous Hall effect in collinear antiferromagnets, Sci. Adv. **6**, eaaz8809 (2020).

[7] L.-D. Yuan, Z. Wang, J.-W. Luo, E. I. Rashba, and A. Zunger, Giant momentum-dependent spin splitting in centrosymmetric low-Z antiferromagnets, Phys. Rev. B **102**, 014422 (2020).

[8] I. Mazin, Altermagnetism in MnTe: Origin, predicted manifestations, and routes to detwinning, Phys. Rev. B **107**, L100418 (2023).

[9] R. M. Fernandes, V. S. de Carvalho, T. Birol, and R. G. Pereira, Topological transition from nodal to nodeless Zeeman splitting in altermagnets, Phys. Rev. B **109**, 024404 (2024).

[10] B. Brekke, A. Brataas, and A. Sudbø, Two-dimensional altermagnets: Superconductivity in a minimal microscopic model, Phys. Rev. B **108**, 224421 (2023).

[11] Y.-X. Li and C.-C. Liu, Majorana corner modes and tunable patterns in an altermagnet heterostructure, Phys. Rev. B **108**, 205410 (2023).

[12] S.-W. Cheong and F.-T. Huang, Altermagnetism with noncollinear spins, npj Quantum Mater. **9**, 13 (2024).

[13] Y. S. Ang, Altermagnetic Schottky contact, arXiv:2310.11289.

[14] C. Autieri, R. M. Sattigeri, G. Cuono, and A. Fakhredin, Dzyaloshinskii-Moriya interaction inducing weak ferromagnetism in centrosymmetric altermagnets and weak ferrimagnetism in noncentrosymmetric altermagnets, arXiv:2312.07678.

[15] L. Šmejkal, A. Marmodoro, K.-H. Ahn, R. González-Hernández, I. Turek, S. Mankovsky, H. Ebert, S. W. D'Souza, O. Šipr, J. Sinova *et al.*, Chiral magnons in altermagnetic RuO₂, Phys. Rev. Lett. **131**, 256703 (2023).

[16] M. Wei, L. Xiang, F. Xu, L. Zhang, G. Tang, and J. Wang, Gapless superconducting state and mirage gap in altermagnets, Phys. Rev. B **109**, L201404 (2024).

[17] P. A. McClarty and J. G. Rau, Landau theory of altermagnetism, Phys. Rev. Lett. **132**, 176702 (2024).

[18] D. S. Antonenko, R. M. Fernandes, and J. W. Venderbos, Mirror Chern bands and Weyl nodal loops in altermagnets, arXiv:2402.10201.

[19] S. A. A. Ghorashi, T. L. Hughes, and J. Cano, Altermagnetic routes to Majorana modes in zero net magnetization, arXiv:2306.09413.

[20] C. Sun, A. Brataas, and J. Linder, Andreev reflection in altermagnets, Phys. Rev. B **108**, 054511 (2023).

[21] T. A. Maier and S. Okamoto, Weak-coupling theory of neutron scattering as a probe of altermagnetism, Phys. Rev. B **108**, L100402 (2023).

[22] T. Sato, S. Haddad, I. C. Fulga, F. F. Assaad, and J. van den Brink, Altermagnetic anomalous Hall effect emerging from electronic correlations, arXiv:2312.16290.

[23] I. Turek, Altermagnetism and magnetic groups with pseudoscalar electron spin, Phys. Rev. B **106**, 094432 (2022).

[24] J. A. Ouassou, A. Brataas, and J. Linder, dc Josephson effect in altermagnets, Phys. Rev. Lett. **131**, 076003 (2023).

[25] P. Das, V. Leeb, J. Knolle, and M. Knap, Realizing altermagnetism in Fermi-Hubbard models with ultracold atoms, Phys. Rev. Lett. **132**, 263402 (2024).

[26] A. Fakhredine, R. M. Sattigeri, G. Cuono, and C. Autieri, Interplay between altermagnetism and nonsymmorphic symmetries generating large anomalous Hall conductivity by semi-Dirac points induced anticrossings, Phys. Rev. B **108**, 115138 (2023).

[27] Y. Fang, J. Cano, and S. A. A. Ghorashi, Quantum geometry induced nonlinear transport in altermagnets, arXiv:2310.11489.

[28] V. Leeb, A. Mook, L. Šmejkal, and J. Knolle, Spontaneous formation of altermagnetism from orbital ordering, Phys. Rev. Lett. **132**, 236701 (2024).

[29] I. Mazin, R. González-Hernández, and L. Šmejkal, Induced monolayer altermagnetism in MnP(S,Se)₃ and FeSe, arXiv:2309.02355.

[30] M. Roig, A. Kreisel, Y. Yu, B. M. Andersen, and D. F. Agterberg, Minimal models for altermagnetism, arXiv:2402.15616.

[31] F. Bernardini, M. Fiebig, and A. Cano, Ruddlesden-Popper and perovskite phases as a material platform for altermagnetism, arXiv:2401.12910.

[32] S. Qu, Z.-F. Gao, H. Sun, K. Liu, P.-J. Guo, and Z.-Y. Lu, Extremely strong spin-orbit coupling effect in light element altermagnetic materials, arXiv:2401.11065.

[33] G. Diniz and E. Vernek, Suppressed Kondo screening in two-dimensional altermagnets, Phys. Rev. B **109**, 155127 (2024).

[34] J. Sødequist and T. Olsen, Two-dimensional altermagnets from high throughput computational screening: Symmetry requirements, chiral magnons and spin-orbit effects, Appl. Phys. Lett. **124**, 182409 (2024).

[35] Y.-L. Lee, Magnetic impurities in an altermagnetic metal, arXiv:2312.15733.

[36] P.-J. Guo, Y. Gu, Z.-F. Gao, and Z.-Y. Lu, Altermagnetic ferroelectric LiFe₂F₆ and spin-triplet excitonic insulator phase, arXiv:2312.13911.

[37] D. Chakraborty and A. M. Black-Schaffer, Zero-field finite-momentum and field-induced superconductivity in altermagnets, Phys. Rev. B **110**, L060508 (2024).

[38] B. Chi, L. Jiang, Y. Zhu, G. Yu, C. Wan, J. Zhang, and X. Han, Crystal-facet-oriented altermagnets for detecting ferromagnetic and antiferromagnetic states by giant tunneling magnetoresistance, Phys. Rev. Appl. **21**, 034038 (2024).

[39] Y. Zhao, Y. Jiang, H. Bae, K. Das, Y. Li, C.-X. Liu, and B. Yan, Hybrid-order topology in unconventional magnets of Eu-based Zintl compounds with surface-dependent quantum geometry, arXiv:2403.06304.

[40] L. Šmejkal, A. H. MacDonald, J. Sinova, S. Nakatsuji, and T. Jungwirth, Anomalous Hall antiferromagnets, Nat. Rev. Mater. **7**, 482 (2022).

[41] Z. Feng, X. Zhou, L. Šmejkal, L. Wu, Z. Zhu, H. Guo, R. González-Hernández, X. Wang, H. Yan, P. Qin *et al.*, An anomalous Hall effect in altermagnetic ruthenium dioxide, Nat. Electron. **5**, 735 (2022).

[42] M. Leiviskä, J. Rial, A. Bad'ura, R. Lopes Seeger, I. Kounta, S. Beckert, D. Kriegner, I. Joumard, E. Schmoranzerová, J. Sinova

et al., Anisotropy of the anomalous Hall effect in thin films of the altermagnet candidate Mn_5Si_3, Phys. Rev. B **109**, 224430 (2024).

[43] X. Zhou, W. Feng, R.-W. Zhang, L. Šmejkal, J. Sinova, Y. Mokrousov, and Y. Yao, Crystal thermal transport in altermagnetic RuO_2, Phys. Rev. Lett. **132**, 056701 (2024).

[44] S. Lee, S. Lee, S. Jung, J. Jung, D. Kim, Y. Lee, B. Seok, J. Kim, B. G. Park, L. Šmejkal *et al.*, Broken Kramers degeneracy in altermagnetic MnTe, Phys. Rev. Lett. **132**, 036702 (2024).

[45] J. Krempaský, L. Šmejkal, S. D'Souza, M. Hajlaoui, G. Springholz, K. Uhlířová, F. Alarab, P. Constantinou, V. Strocov, D. Usanov *et al.*, Altermagnetic lifting of Kramers spin degeneracy, Nature (London) **626**, 517 (2024).

[46] Y.-P. Zhu, X. Chen, X.-R. Liu, Y. Liu, P. Liu, H. Zha, G. Qu, C. Hong, J. Li, Z. Jiang *et al.*, Observation of plaid-like spin splitting in a noncoplanar antiferromagnet, Nature (London) **626**, 523 (2024).

[47] O. Fedchenko, J. Minár, A. Akashdeep, S. W. D'Souza, D. Vasilyev, O. Tkach, L. Odenbreit, Q. Nguyen, D. Kutnyakhov, N. Wind *et al.*, Observation of time-reversal symmetry breaking in the band structure of altermagnetic RuO_2, Sci. Adv. **10**, eadj4883 (2024).

[48] S. Reimers, L. Odenbreit, L. Šmejkal, V. N. Strocov, P. Constantinou, A. B. Hellenes, R. J. Ubiergo, W. H. Campos, V. K. Bharadwaj, A. Chakraborty *et al.*, Direct observation of altermagnetic band splitting in CrSb thin films, Nat. Commun. **15**, 2116 (2024).

[49] R. S. K. Mong, A. M. Essin, and J. E. Moore, Antiferromagnetic topological insulators, Phys. Rev. B **81**, 245209 (2010).

[50] J. Liu, T. H. Hsieh, P. Wei, W. Duan, J. Moodera, and L. Fu, Spin-filtered edge states with an electrically tunable gap in a two-dimensional topological crystalline insulator, Nat. Mater. **13**, 178 (2014).

[51] Y.-R. Ding, D.-H. Xu, C.-Z. Chen, and X. Xie, Hinged quantum spin Hall effect in antiferromagnetic topological insulators, Phys. Rev. B **101**, 041404(R) (2020).

[52] X. Hu, N. Mao, H. Wang, Y. Dai, B. Huang, and C. Niu, Quantum spin Hall effect in antiferromagnetic topological heterobilayers, Phys. Rev. B **103**, 085109 (2021).

[53] Y. Xue, W. Xu, B. Zhao, J. Zhang, and Z. Yang, Antiferromagnetic quantum spin Hall insulators with high spin Chern numbers, Phys. Rev. B **108**, 075138 (2023).

[54] Y. Yang, Z. Xu, L. Sheng, B. Wang, D. Y. Xing, and D. N. Sheng, Time-reversal-symmetry-broken quantum spin Hall effect, Phys. Rev. Lett. **107**, 066602 (2011).

[55] P. Liu, J. Li, J. Han, X. Wan, and Q. Liu, Spin-group symmetry in magnetic materials with negligible spin-orbit coupling, Phys. Rev. X **12**, 021016 (2022).

[56] J. Yang, Z.-X. Liu, and C. Fang, Symmetry invariants in magnetically ordered systems having weak spin-orbit coupling, arXiv:2105.12738.

[57] Z. Xiao, J. Zhao, Y. Li, R. Shindou, and Z.-D. Song, Spin space groups: Full classification and applications, arXiv:2307.10364.

[58] X.-L. Qi and S.-C. Zhang, Topological insulators and superconductors, Rev. Mod. Phys. **83**, 1057 (2011).

[59] M. Z. Hasan and C. L. Kane, *Colloquium*: Topological insulators, Rev. Mod. Phys. **82**, 3045 (2010).

[60] D. Xiao, G.-B. Liu, W. Feng, X. Xu, and W. Yao, Coupled spin and valley physics in monolayers of MoS_2 and other group-VI dichalcogenides, Phys. Rev. Lett. **108**, 196802 (2012).

[61] S. Zhang, K. Bian, and Y. Jiang, Perspective: Nanoscale electric sensing and imaging based on quantum sensors, Quantum Frontiers **2**, 19 (2023).

[62] H.-Y. Ma, D. Guan, S. Wang, Y. Li, C. Liu, H. Zheng, and J.-F. Jia, Quantum spin Hall and quantum anomalous Hall states in magnetic Ti_2Te_2O single layer, J. Phys.: Condens. Matter **33**, 21LT01 (2021).